## 6 *EXPERIMENTAL DETAILS*

ORNL/TM--11671

DE91 000871

Engineering Physics and Mathematics Division

# CROSS SECTIONS FOR PRODUCTION OF 70 DISCRETE-ENERGY GAMMA RAYS CREATED BY NEUTRON INTERACTIONS WITH $^{56}$Fe FOR $E_n$ to 40 MeV: TABULATED DATA

J. K. Dickens, J. H. Todd, and D. C. Larson

DATE PUBLISHED — September 1990

Prepared for the
Office Energy Research
Division of Nuclear Physics

Prepared by the
OAK RIDGE NATIONAL LABORATORY
Oak Ridge, Tennessee 37831
operated by
MARTIN MARIETTA ENERGY SYSTEMS, INC.
for the
U.S. DEPARTMENT OF ENERGY
under contract DE–AC05–84OR21400

# CONTENTS

# LIST OF FIGURES

# LIST OF TABLES

# ACKNOWLEDGMENTS

We express our appreciation to C. Y. Fu and D. M. Hetrick for illuminating discussions about the ENDF/B-6 evaluation, to R. L. Shannon and to K. J. Northcutt (Analytical Chemistry Division) for careful preparation of the $^{56}Fe$ samples in the polyethylene containers, to H. A. Todd and T. A. Lewis and the ORELA operators for efficient and capable accelerator operation, to K. M. Wallace for careful radiation monitoring of our experimental area, and to S. Damewood for her detailed effort required in the preparation of the manuscript of this report.

# ABSTRACT

Inelastic and nonelastic neutron interactions with $^{56}$Fe have been studied for incident neutron energies between 0.8 and 41 MeV. An iron sample isotopically enriched in the mass 56 isotope was used. Gamma rays representing 70 transitions among levels in residual nuclei were identified, and production cross sections were deduced. The reactions studied were $^{56}\mathrm{Fe}(n,n')^{56}\mathrm{Fe}$, $^{56}\mathrm{Fe}(n,p)^{56}\mathrm{Mn}$, $^{56}\mathrm{Fe}(n,2n)^{55}\mathrm{Fe}$, $^{56}\mathrm{Fe}(n,d+n,np)^{55}\mathrm{Mn}$, $^{56}\mathrm{Fe}(n,t+n,nd+n,2np)^{54}\mathrm{Mn}$, $^{56}\mathrm{Fe}(n,\alpha)^{53}\mathrm{Cr}$, $^{56}\mathrm{Fe}(n,n\alpha)^{52}\mathrm{Cr}$, and $^{56}\mathrm{Fe}(n,3n)^{54}\mathrm{Fe}$. Values obtained for production cross sections as functions of incident neutron energy are presented in tabular form.

# 1. INTRODUCTION

As part of a continuing program[1-4] to provide discrete-energy gamma-ray production cross sections for applied needs, we have measured cross sections for gamma rays representing 70 transitions among the residual nuclei $^{56}$Fe, $^{56}$Mn, $^{55}$Fe, $^{55}$Mn, $^{54}$Fe, $^{54}$Mn, $^{53}$Cr, and $^{52}$Cr created by neutrons incident on an isotopically enriched sample of $^{56}$Fe. Neutron energies spanned the incident energy region between threshold and 41 MeV. The emphasis for this experiment was on the observation and measurement of tertiary reactions listed since there are in the literature a number of reports[5-19] on inelastic scattering gamma-ray production. Data reduced for inelastic scattering gamma-ray production for incident neutron energies up to 20 MeV in the present experiment are not as extensive as already reported; these data serve primarily to serve as a measure of the reliability of the present measurements. Inelastic-scattering data for incident neutron energies between 22 and 41 MeV, however, are new, and they can be utilized to estimate total inelastic-scattering cross sections for neutron interactions with $^{56}$Fe for these more energetic incident neutrons.

## 2. EXPERIMENTAL DETAILS

The general experimental configuration has been discussed previously;[1,4] we present here a brief description and some details pertaining to the particular sample used, $^{56}$Fe.

Neutrons of energies up to 41 MeV[20] were obtained from the Oak Ridge Electron Linear Accelerator (ORELA) facility. The ORELA was operated at 800 pulses/s, and each beam burst was ~15 ns in duration. The pulsed electrons struck a tantalum convertor creating bremsstrahlung, and the bremsstrahlung struck a block of beryllium creating a "white" spectrum of neutrons. The neutrons traveled about 20 m through an evacuated tube to the experimental area. The neutron fluence/unit energy interval from the beryllium peaks at about 1 MeV[21] and decreases at higher neutron energies; there is still a sufficient flux at $E_n \sim 40$ MeV to obtain adequate statistical accuracy for the principal gamma rays observed in this experiment. As illustrated in Fig. 1 a small monitor detector was set to intercept the beam after it left the vacuum. The beam flux *vis-a-vis* this monitor was calibrated in a manner similar to an earlier calibration already documented[22] except that the new detector-response program SCINFUL[23] was used rather than the older code O5S[24] which had been used in the earlier work. The neutrons traveled an additional 2 m before striking a sample described below containing the isotope $^{56}$Fe. The neutron beam then reentered an evacuated tube and continued another 10 m into a paraffin-shielded beam dump. A scan of the beam profile at the sample position was done using a small (~1 cm$^3$) NE-110 scintillator. The scan was along both a horizontal and a vertical diameter, and to within the statistical uncertainties of the measurements, the incident neutron beam was found to be uniform.

Gamma rays created by interactions of the incident neutrons with the isotope $^{56}$Fe were detected using a high-resolution intrinsic Germanium detector. This detector had a volume of ~150 cm$^3$, and its resolution for detection of 1-MeV gamma rays was ~2 keV. The purpose of the electronics was to (a) provide a fast pulse to measure the time of the event with respect to the time representing the initiation of the linac pulse; from this information was deduced the energy of the neutron which interacted with the sample isotope yielding the detected gamma ray; and (b) a linear and amplified voltage pulse from which was deduced the energy of the gamma ray created by the interaction.

The sample material was obtained from the DOE pool of stable isotopes. It was from batch no. 154901, and was enriched 99.93% in the isotope $^{56}$Fe. The only other elements given in the data sheet supplied with the sample were Ca and Cu at 0.01% each, and Si at 0.1%. The sample material was supplied to us as a powdered metal. Because of the expense involved, it was decided not to have the sample recast as a single solid piece. Instead, sample material was encapsulated in 41 small (0.9 cm diam by 1.8 cm high) polyethylene cylinders. Each capsule held about 1.5 gm of the Fe powder. The capsules were then lightly glued together in two layers as exhibited in Fig. 2, and the two layers were lightly glued together (with the 21-capsule layer upstream of the 20-capsule layer) and then mounted in a cardboard sample holder. The sample was placed at 45 deg with respect to the incident neutron beam so that the ovate shape of the sample roughly approximated a circle from the viewpoint of the incident beam. The total $^{56}$Fe mass was 62.75 gm.

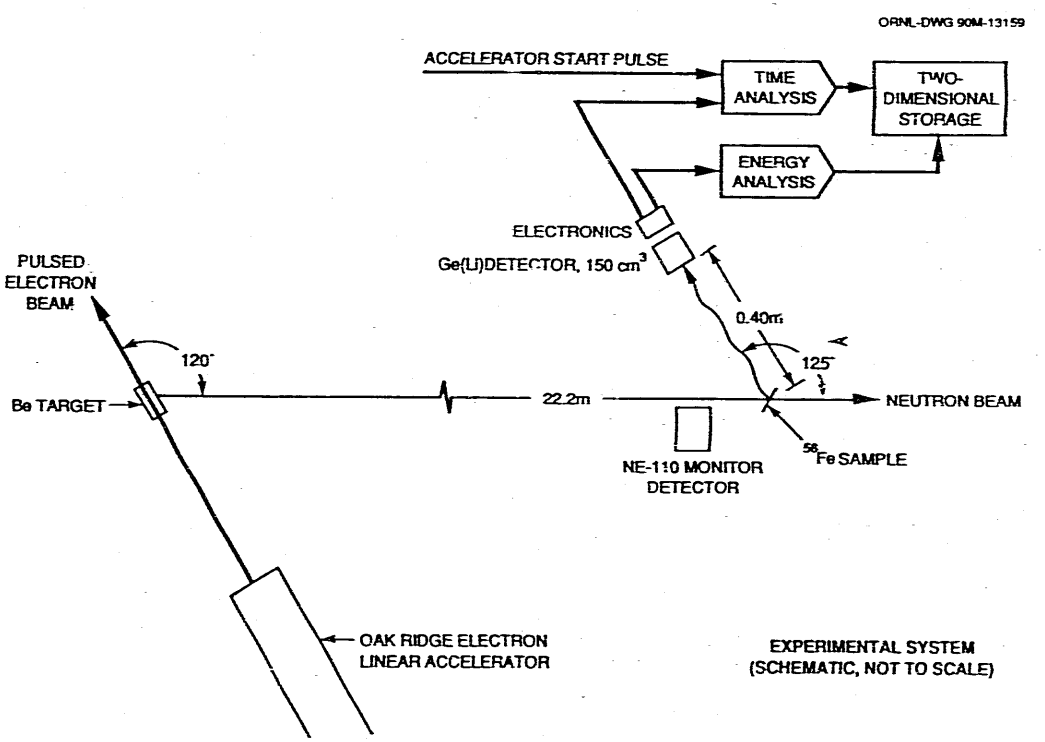


Fig. 1. Schematic representation of the experimental system.

ORNL-DWG 90M-12714

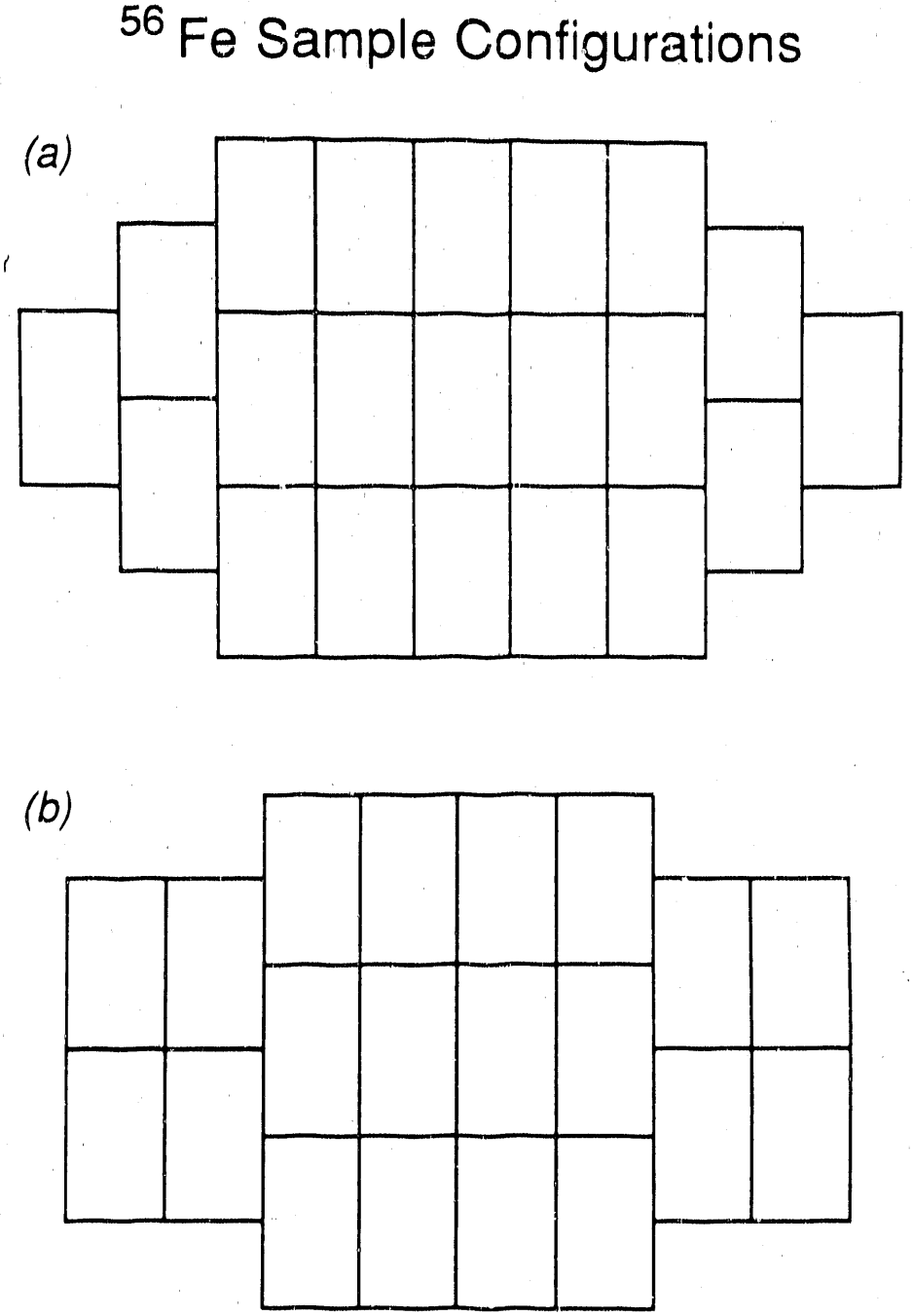


**Fig. 2. Sample configuration.** The upper configuration (A) exhibits the planar placement of 21 iron-powder filled cylindrical polyethylene capsules, each 1-cm diameter by 2-cm height. The lower configuration (B) exhibits the placement of 20 capsules. The total sample was formed by placing the (B) configuration behind the (A) configuration as seen by the incident neutron beam with (B) offset by a cylinder radius as schematically indicated in the figure. The plane of this total sample was then placed at 45 deg with respect to the direction of the incident beam, i.e., with the sample normal offset by 10 deg with respect to the sample-to-detector direction, so that the approximate ovate shape of the sample roughly coincided with the circular shape of the impinging neutron beam.

A "background" sample containing 21 empty capsules and having a polyethylene mass of about 9 gm was similarly fabricated and used to estimate the amount of gamma-ray production from the capsule material in the sample.

Data were accumulated in a SEL 810B computer in a three-dimensional array, namely, timing information vs pulse-height information vs yield. In this matter 31 gamma-ray pulse-height spectra[25] were accumulated, each for a pre-determined interval of the time following the ORELA beam burst. The timing information was later converted to the energy of the neutron responsible for the detected event. The spectrum obtained for the incident neutron energy interval 27.1–29.4 MeV is shown in Fig. 3. In this spectrum are observed gamma rays due to transitions among seven of the eight residual isotopes reported on herein; only the $^{56}$Fe$(n,\alpha)^{53}$Cr reaction is not observed at this $E_n$. Data accumulated in the SEL 810B computer were transferred to a VAX 11/785 computer in the FORODF[26] format for off-line data analysis. Data were acquired over a period of about three weeks of ORELA operation. Individual runs were corrected for dead time and overflows and were then summed. Data analysis consisted of an initial preparation of the data using the code PRPGE;[27] this step broke up the long FORODF data file into blocks representing the individual spectra, with a header block containing needed information specific to the individual spectrum (i.e., incident neutron energy, incident integrated flux for the given neutron energy bin, etc.). In this manner, a long, binary file was created which served as input to the program GRPGLI.[28] This program analyzed each spectrum for peaks and peak yields, converted the peak centroids to gamma-ray energies and then converted the peak yields to efficiency-corrected gamma-ray yields and then to gamma-ray production cross sections. Then, using a table look-up process, the program assigned gamma-ray peaks to the responsible isotope(s), checking, for example, reaction thresholds (supplied in the table) as aids in assignments. Our experience with GRPGLI is that the program adequately analyzes large-yield peaks (e.g., $E_\gamma$ = 156 keV in Fig. 3) and it does reasonably well with small-yield peaks (e.g., $E_\gamma$ = 308 keV in Fig. 3) when it identifies them, but it often misses entirely small-yield peaks. Therefore, for gamma rays from *expected* transitions, the program is requested to review the data in the region of the expected gamma ray and provide an estimate of the "yield" for a "peak" centered at the desired energy. For most cases the program indicates correctly the presence or absence of small peaks but in about 25% of the cases it has been necessary to redo the analysis using an interactive code called PLOTDATA written for an IBM-AT PC system[29] to obtain more accurate yields. Data were reduced for altogether 70 separate gamma rays representing 72 transitions (two transitions having essentially identical energies), and the 70 gamma rays are tabulated in Table 1 in a manner to quickly identify the responsible isotope and excited energy level.

Cross-section data were corrected for (a) absorption of gamma radiation by the sample, (b) attenuation of the incident neutron beam, and (c) multiple scattering of the incident neutrons in the sample. The absorption correction was straightforward using published gamma-ray absorption data[30] and ranged from 4% for high-energy gamma rays to 25% for $E_\gamma$ = 126 keV. Corrections to the data for beam attenuation and multiple scattering were accomplished using a Monte Carlo program named IRON adapted from the documented Monte Carlo program SCINFUL.[23] The program IRON required input cross sections for the various reactions of interest; these were obtained from the draft version of ENDF/B-6 for Fe for $E_n \leq 20$ MeV.[31] For 20 MeV $< E_n \leq 41$ MeV, cross sections were adapted from the eval-

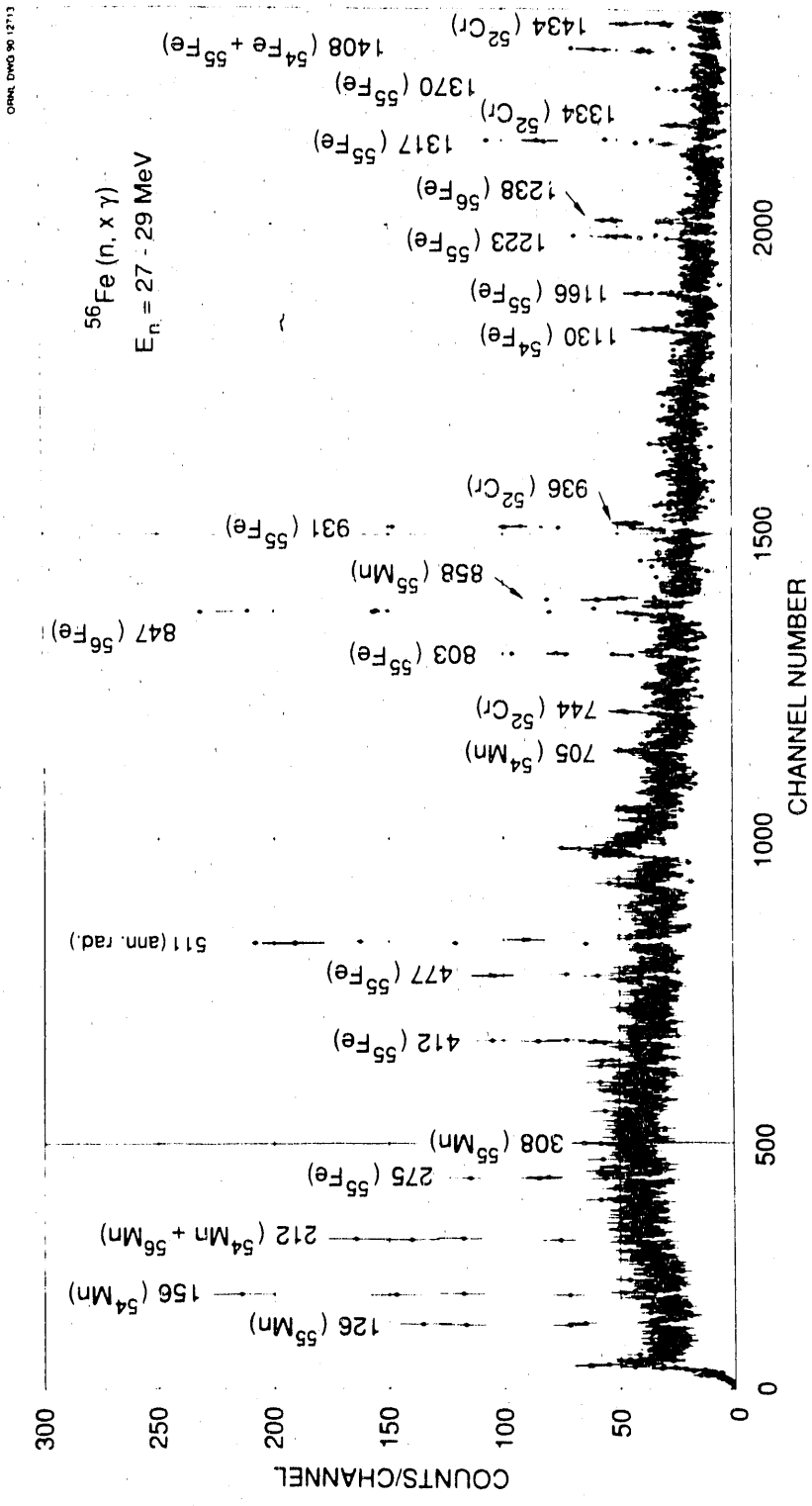


**Fig. 3. Pulse-height spectrum for 27 to 29 MeV neutron interactions with the $^{56}$Fe sample.** Gamma-ray peaks are labeled by the gamma-ray energy (keV) and the symbol of the residual nucleus. The experimental dispersion is ~0.6 keV/channel.

Table 1. Gamma rays for which production cross sections are tabulated in this report

| $E_\gamma$ (keV) | Reaction(s) and excited states (keV) | | | | | | | |
|---|---|---|---|---|---|---|---|---|
| | $(n,n')^{56}$Fe | $(n,p)^{56}$Mn | $(n,\alpha)^{53}$Cr | $(n,d)+(n,np)^{55}$Mn | $(n,t)+(n,2np)^{54}$Mn | $(n,2n)^{55}$Fe | $(n,3n)^{54}$Fe | $(n,n\alpha)^{52}$Cr |
| 126 | | | | 126 | | | | |
| 156 | | | | | 156 | | | |
| 212 | | 212 | | | 368 | | | |
| 247 | | | 1537 | | | | | |
| 251 | | | | | 407 | | | |
| 271 | | 486 | | | | | | |
| 275 | | | | | | 2814 | | |
| 308 | | | | 1292[a] | | | | |
| 314 | | 341 | | | | | | |
| 336 | | 336 | | | | | | |
| 385 | | | | | | 1317 | | |
| 412 | | | | | | 412 | | |
| 454 | | 454 | | | | | | |
| 477 | | | | | | 1408 | | |
| 530 | | | 1537 | | | | | |
| 533 | | | | | | 3072 | | |
| 541 | | 753 | | | | | | |
| 564 | | | 564 | | | | | |
| 705 | | | | | 1073 | | | |
| 744 | | | | | | | | 3114 |
| 757 | | | | | | | 3295 | |
| 772 | | | | | | 2984 | | |
| 803 | | | | | | 2212 | | |
| 827 | | | | | | 2144 | | |
| 847 | 847 | | | | | | | |
| 858 | | | | 984 | | | | |
| 883 | | | 2172 | | | | | |
| 831 | | | | | | 931 | | |
| 936 | | | | | | | | 2370 |
| 985 | | | | | | 2301 | | |
| 1007 | | | 1007 | | | | | |
| 1019 | | | | 2312 | | | | |
| 1038 | 3123 | | | | | | | |
| 1130 | | | | | | | 2538 | |
| 1166 | | | | 1292[a] | | | | |

Table 1. Continued

| $E_\gamma$ (keV) | Reaction(s) and excited states (keV) | | | | | | | |
|---|---|---|---|---|---|---|---|---|
| | $(n,n')^{56}$Fe | $(n,p)^{56}$Mn | $(n,\alpha)^{53}$Cr | $(n,d)$ + $(n,np)^{55}$Mn | $(n,t)$ + $(n,2np)^{54}$Mn | $(n,2n)^{55}$Fe | $(n,3n)^{54}$Fe | $(n,n\alpha)^{52}$Cr |
| 1213 | | | | | | 2144 | | |
| 1223 | | | | | | 2539 | | |
| 1238 | 2035 | | | | | | | |
| 1290 | | | 1290 | | | | | |
| 1293 | | | | 1293[a] | | | | |
| 1303 | 3388 | | | | | | | |
| 1317 | | | | | | 1317 | | |
| 1334 | | | | | | | | 2768 |
| 1370 | | | | | | 2301 | | |
| 1408 | | | | | | 1408 | 1408 | |
| 1434 | | | | | | | | 1434 |
| 1447 | | | 2453 | | | | | |
| 1507 | | | | | | 1918 | | |
| 1528 | | | | 1528 | | | | |
| 1556 | | | | | | 2872 | | |
| 1576 | | | | | | 2984 | | |
| 1622 | | | | | | 2939 | | |
| 1641[b] | | | | | | 2052 | | |
| 1649 | | | 2656 | | | | | |
| 1669 | 3755 | | | | | | | |
| 1792 | | | | | | 3109 | | |
| 1811 | 2658 | | | | | | | |
| 1918 | | | | | | 1918 | | |
| 1974 | | | 1974 | | | | | |
| 2035 | 4120 | | | | | | | |
| 2052 | | | | | | 2052 | | |
| 2058 | | | | | | 2470 | | |
| 2095 | 2942 | | | | | | | |
| 2113 | 2960 | | | | | | | |
| 2144[b] | | | | | | 2144 | | |
| 2178 | | | | | | 3109 | | |
| 2198 | | | | 2198 | | | | |
| 2273 | 3120 | | | | | | | |
| 2321 | | | 2321 | | | | | |
| 2470 | | | | | | 2470 | | |

[a] Separate levels at $E_x$ = 1292 and 1293 keV.

[b] Only an upper limit to the production cross section is given.

uation of Arthur and Young.[32] Inelastic scattering cross sections were supplied for individual levels up to $E_x = 3.449$ MeV, and a "continuum" cross section was given to represent scattering into higher excited states of $^{56}$Fe. Gamma-ray branching ratios[33] had to be included, also, with estimates for decay of the "continuum." Input cross sections were tabulated point wise with (usually) log-log interpolation; these data were checked ahead of time for accuracy by calculating the neutron + Fe total cross sections at many neutron energies between 1 and 40 MeV. It was not possible to model exactly the sample as described above. Instead the sample was treated as a disk made up of a homogeneous mixture of Fe, C and H. Angular distributions of scattered neutrons were included for scattering from C and H taken from the SCINFUL code; for Fe the elastic scattering angular distribution information was taken from ENDF/B-6. The remaining neutron scattering reactions were taken as isotropic in the center of mass. All scattering computations were done relativistically. The incident neutron was followed as it scattered in the sample until it was either absorbed or it escaped from the sample. The program provided the multiple-scattering estimate to the neutron attenuation which could be checked against a simple computation using the total cross section for the mixed sample. These attenuation corrections ranged from 4% to 15%. The program then supplied the *total* correction for both neutron attenuation and multiple scattering, and these values had substantial variations dependent upon gamma-ray energy as well as the incident neutron energy. The values of the factors needed to multiply the GRPGLI-generated production cross sections ranged from about 0.5 to 1.1. Clearly the usual assumption[34] that the multiple scattering approximately compensates for the neutron attenuation in a "thin" sample is inadequate for the present measurements.

Uncertainties, for the most part, were dominated by the statistical uncertainties of the yields of the raw peaks in the spectral data. However, systematic uncertainties were computed and combined in the final data analysis. These included uncertainties in detector efficiency (see Table 2 for a complete tabulation of uncertainties vs $E_\gamma$) and uncertainties in the incident beam flux (see Table 3 for a complete tabulation of uncertainties vs $E_n$ bin). Uncertainties in the above-discussed Monte Carlo estimates of neutron-attenuation and multiple-scattering corrections were based on number of "events" calculated by the code for each gamma ray at each incident $E_n$ bin before and after the correction. These uncertainties were, for most cases, $\leq$5% of the correction, and in all cases were smaller than the statistical uncertainties of the raw peaks in the spectral data.

There was one other important correction that had to be computed and that was for time slewing (i.e., electronic "walk"). At the beginning of the experiment we determined that our detector and electronics exhibited an overall time resolution of $\approx 8$ ns for $E_\gamma = 511$ keV. Some adjustments were made to the electronics to somewhat improve the timing resolution, especially for $E_\gamma = 847$ keV, but the system was not tuned especially for the much smaller-energy gamma rays at the beginning of the experiment. However, the spectra exhibited unexpectedly good yields for low-energy gamma rays. As it happened data reduction commenced after the $^{56}$Fe sample had been returned to the pool. As a part of the data reduction the timing of the system was studied as a function of $E_\gamma$ as the energy was decreased below 0.5 MeV. The timing resolution worsened moderately as expected with decreasing gamma-ray energy; however, as $E_\gamma$ was decreased below 0.3 MeV the centroid of the timing peak shifted toward longer times and the timing resolution worsened

Table 2. Uncertainties assigned to gamma-ray detection efficiency

| Gamma-ray energy (keV) | Uncertainty (%) | Gamma-ray energy (keV) | Uncertainty (%) |
|---|---|---|---|
| 126–1334 | 3.0 | 1811 | 4.9 |
| 1370 | 3.1 | 1918 | 5.3 |
| 1408 | 3.3 | 1974 | 5.4 |
| 1434 | 3.4 | 2035 | 5.6 |
| 1447 | 3.4 | 2052 | 5.7 |
| 1507 | 3.7 | 2058 | 5.7 |
| 1528 | 3.8 | 2095 | 5.8 |
| 1556 | 3.9 | 2113 | 5.9 |
| 1576 | 4.0 | 2144 | 6.0 |
| 1622 | 4.1 | 2178 | 6.1 |
| 1641 | 4.2 | 2198 | 6.2 |
| 1649 | 4.2 | 2273 | 6.4 |
| 1669 | 4.3 | 2321 | 6.6 |
| 1792 | 4.8 | 2470 | 7.0 |

Table 3. Uncertainty in incident neutron beam flux for each neutron bin

| Incident $E_n$ (MeV) | Uncertainty (%) | Incident $E_n$ (MeV) | Uncertainty (%) |
|---|---|---|---|
| 0.86 – 0.91 | 23.8 | 11.28 – 12.09 | 4.7 |
| 0.91 – 0.98 | 18.6 | 12.09 – 12.98 | 3.65 |
| 0.98 – 1.16 | 10.0 | 12.98 – 13.97 | 3.02 |
| 1.16 – 1.68 | 5.3 | 13.97 – 15.09 | 2.85 |
| 1.68 – 2.36 | 6.7 | 15.09 – 16.69 | 2.38 |
| 2.36 – 3.07 | 5.8 | 16.69 – 18.55 | 2.20 |
| 3.07 – 3.83 | 6.9 | 18.55 – 20.76 | 2.03 |
| 3.83 – 4.71 | 5.0 | 20.76 – 22.82 | 2.26 |
| 4.71 – 5.65 | 4.2 | 22.82 – 25.20 | 2.22 |
| 5.65 – 6.56 | 5.4 | 25.20 – 27.99 | 2.25 |
| 6.56 – 7.49 | 6.1 | 27.99 – 30.40 | 2.27 |
| 7.49 – 8.26 | 6.5 | 30.40 – 33.15 | 2.55 |
| 8.26 – 9.02 | 6.5 | 33.15 – 36.29 | 2.80 |
| 9.02 – 9.90 | 6.2 | 36.29 – 28.64 | 5.5 |
| 9.90 – 10.56 | 6.2 | 38.64 – 41.23 | 8.2 |
| 10.56 – 11.28 | 4.1 | | |

more rapidly than reported[35,36] for other similar germanium detector systems. Finally, for $E_\gamma = 122$ keV (obtained using an $^{152}$Eu source) the timing resolution was ≈30 ns; the timing spectrum at this energy, however, exhibited a substantial non-Gaussian "tail" extending to times >200 ns.[37] Since these times were considerably longer than the chosen experimental time intervals it was necessary to develop a program to estimate the corrections due to these broad timing characteristics. The program that was developed was an iterative program designed to compute a postu-

lated set of yields, one for each experimental time bin, of the gamma ray in question which, when the overall timing spectrum for that gamma ray was folded in with the experimental timing bin structure, resulted in the observed set of yields. Corrections were computed for the data for all of the principal gamma rays. Corrections for $E_\gamma = 847$ keV were a few percent for $E_n \leq 14$ MeV, and increased to $\approx$20% for $E_n \sim 25$ MeV (where the width of the time bin was nominally 16 ns). For $E_\gamma = 126$ keV, however, the correction was a factor of 3.0 for $E_n \sim 35$ MeV. Estimates for the uncertainty in each such correction were made based primarily upon reproducibility of the computed results by varying (within uncertainties) the initial GRPGLI yields. Essentially in every instance the uncertainty on the estimated correction due to time slewing was not the dominant uncertainty.

Each of two gamma rays, namely $E_\gamma = 212$ keV and 1408 keV, resulted from (the summing of) transitions in two separate residual nuclides. For each gamma ray, cross sections are reported for the reaction with the smaller threshold only up to the threshold energy for the "other" reaction. Then for the "other" reaction cross sections were determined by first obtaining the total cross section for the gamma ray and then subtracting an estimate due to the contribution from the reaction having the smaller threshold. For example, for $E_\gamma = 1408$ keV, the two transitions are in $^{55}$Fe and $^{54}$Fe, and the two thresholds are, respectively, 12.83 and 22.30 MeV. Hence, production cross sections are reported for $^{55}$Fe for $E_n$ only up to 22.8 MeV. The determination of production cross sections for the 1408-keV transition in $^{54}$Fe is given in Table 4.

A similar situation occurs for $E_\gamma = 411$ keV, but in this case we did not attempt to deduce production cross sections for the higher threshold nuclide, $^{54}$Fe.

Production cross sections were obtained for altogether 31 incident neutron energy bins, although, of course, not all of the gamma rays were represented in every neutron energy bin. In addition, for gamma rays having small yields, spectra for two or more neutron-energy bins were sometimes combined so as to obtain better peaks for data reduction. The extracted cross sections are given in tabular form in the next section.

Table 4. Data reduction for $E_\gamma = 1408$ keV: Determining the $^{54}$Fe contribution

| $E_n$ bin (MeV) | $\sigma$ (mb) (total) | Due to $^{55}$Fe[a] | Difference | Adjust[b] | $\sigma(^{54}$Fe) |
|---|---|---|---|---|---|
| 22.8–25.2 | 44.9 ± 4.9 | 44.5 ± 2.8 | 0.4 ± 5.7 | 1.035 | 0.4 ± 5.9 |
| 25.2–28.0 | 57.6 ± 5.6 | 34.4 ± 2.3 | 23.2 ± 6.1 | 1.024 | 23.7 ± 6.2 |
| 28.0–34.0 | 85.2 ± 7.6 | 27.9 ± 3.5 | 57.3 ± 8.4 | 1.014 | 58.1 ± 8.5 |
| 34.0–33.2 | 96.7 ± 8.4 | 18.6 ± 3.4 | 78.1 ± 9.1 | 1.018 | 78.9 ± 9.2 |
| 33.2–36.3 | 104.4 ± 8.5 | 14.3 ± 3.4 | 90.1 ± 9.2 | 1.029 | 92.7 ± 9.3 |
| 36.3–38.6 | 93.9 ± 11.0 | 18.3 ± 4.2 | 75.6 ± 11.8 | 1.021 | 77.2 ± 12.0 |
| 38.6–41.2 | 66.1 ± 12.7 | 14.6 ± 3.5 | 51.5 ± 13.1 | 1.030 | 53.0 ± 13.6 |

[a]Obtained from (44/53) × $\sigma(E_\gamma = 477$ keV) for $^{55}$Fe.

[b]Adjustment for different multiple-scattering and attenuation corrections.

# 3. TABULAR PRESENTATION OF THE MEASURED CROSS SECTIONS

Isotopic gamma-ray production cross sections for ten inelastic scattering transitions are tabulated in Tables 5 and 6. The first column of Table 5 lists the binning of the incident neutron energies; this binning was chosen to be comparatively coarse for $E_n \sim 6$ MeV since we were more interested in observing and measuring cross sections for the nonelastic reactions and less interested in the well-measured (at least for $E_n$ up to ~9 MeV and around 14 MeV) inelastic-scattering cross sections.

Table 5. Isotopic gamma-ray production cross sections (mb) for $^{56}Fe(n,n')^{56}Fe$ inelastic scattering reactions

| Incident $E_n$ (MeV) | Gamma-ray energy (keV) of: | | | | |
|---|---|---|---|---|---|
| | 846.8 | 1238.3 | 1810.8 | 2094.5 | 2113.2 |
| 0.86 – 0.91 | 164 ± 40 | | | | |
| 0.91 – 0.98 | 275 ± 52 | | | | |
| 0.98 – 1.16 | 470 ± 49 | | | | |
| 1.16 – 1.68 | 652 ± 37 | | | | |
| 1.68 – 2.36 | 810 ± 55 | 13.1 ± 1.5[a] | | | |
| 2.36 – 3.07 | 961 ± 58 | 73.0 ± 4.8 | 82.7 ± 8.4[b] | | 27.1 ± 8.7[c] |
| 3.07 – 3.83 | 1115 ± 77 | 162.3 ± 11.7 | 167.5 ± 12.6 | 32.0 ± 2.8 | 99.6 ± 7.9 |
| 3.83 – 4.71 | 1180 ± 62 | 238.6 ± 12.8 | 143.6 ± 8.2 | 34.8 ± 3.3 | 103.9 ± 7.2 |
| 4.71 – 5.65 | 1274 ± 57 | 310 ± 14 | 153.6 ± 9.0 | 24.6 ± 2.7 | 100.5 ± 7.0 |
| 5.65 – 6.56 | 1331 ± 90 | 400 ± 30 | 151.7 ± 10.3 | 21.2 ± 3.3 | 90.3 ± 6.8 |
| 6.56 – 7.49 | 1255 ± 79 | 402 ± 26 | 135.1 ± 10.3 | 10.8 ± 2.5 | 64.2 ± 5.2 |
| 7.49 – 8.26 | 1160 ± 79 | 421 ± 28 | 115.0 ± 8.9 | 7.0 ± 2.5 | 48.6 ± 5.2 |
| 8.26 – 9.02 | 1131 ± 75 | 444 ± 31 | 111.0 ± 8.8 | 6.4 ± 2.6 | 47.2 ± 5.1 |
| 9.02 – 9.90 | 1131 ± 72 | 469 ± 32 | 106.2 ± 8.3 | 3.0 ± 1.6 | 52.4 ± 5.3 |
| 9.90 – 10.56 | 1123 ± 72 | 520 ± 36 | 100.0 ± 9.2 | 3.2 ± 2.6 | 54.3 ± 7.8 |
| 10.56 – 11.28 | 1171 ± 52 | 499 ± 23 | 96.9 ± 6.9 | 2.2 ± 1.4 | 49.8 ± 6.0 |
| 11.28 – 12.09 | 1101 ± 54 | 511 ± 26 | 91.3 ± 7.0 | | 30.8 ± 6.9 |
| 12.09 – 12.98 | 947 ± 41 | 490 ± 21 | 80.6 ± 6.8 | | 35.5 ± 6.2 |
| 12.98 – 13.97 | 774 ± 35 | 431 ± 18 | 51.7 ± 5.5 | | 24.8 ± 4.7 |
| 13.97 – 15.09 | 621 ± 29 | 290 ± 16 | 37.5 ± 4.6 | | 15.3 ± 4.7 |
| 15.09 – 16.69 | 409 ± 25 | 193 ± 14 | 30.8 ± 3.9 | | 11.9 ± 2.9 |
| 16.69 – 18.55 | 293 ± 16 | 126.6 ± 8.2 | 21.5 ± 4.1 | | 6.8 ± 3.8 |
| 18.55 – 20.76 | 249 ± 11 | 96.6 ± 5.5 | 10.5 ± 2.8 | | 7.5 ± 4.6 |
| 20.76 – 22.82 | 206.4 ± 9.3 | 63.6 ± 4. | 7.4 ± 3.0 | | 4.5 ± 3.5 |
| 22.82 – 25.20 | 182.5 ± 9.0 | 51.9 ± 4.8 | | | |
| 25.20 – 27.99 | 141.4 ± 8.0 | 43.3 ± 3.8 | | | |
| 27.99 – 30.40 | 122.3 ± 7.9 | 38.3 ± 3.7 | | | |
| 30.40 – 33.15 | 107.9 ± 8.5 | 38.0 ± 4.2 | | | |
| 33.15 – 36.29 | 101.1 ± 7.8 | 33.3 ± 7.1 | | | |
| 36.29 – 38.64 | 89.8 ± 8.8 | 27.6 ± 6.7 | | | |
| 38.64 – 41.23 | 86.0 ± 11.2 | 16.8 ± 4.8 | | | |

[a] For incident neutron energy bin $2.12 \leq E_n \leq 2.36$ MeV.

[b] For incident neutron energy bin $2.71 \leq E_n \leq 3.07$ MeV.

[c] For incident neutron energy bin $3.01 \leq E_n \leq 3.07$ MeV.

Table 6. Isotopic gamma-ray production cross sections (mb) for $^{56}Fe(n,n')^{56}Fe$ inelastic scattering reactions

| Incident $E_n$ (MeV) | Gamma-ray energy (keV) of: | | | | |
|---|---|---|---|---|---|
| | 2273.2 | 1037.9 | 1303.0 | 1609.9 | 2034.9 |
| 3.18 – 3.83 | 56.3 ± 5.7 | 20.6 ± 2.6 | | | |
| 3.83 – 4.71 | 67.8 ± 6.0 | 55.5 ± 3.6 | 3.9 ± 1.4 | | 7.6 ± 1.0[a] |
| 4.71 – 5.65 | 57.5 ± 5.3 | 85.7 ± 5.1 | 11.2 ± 1.5 | 4.8 ± 1.3 | 25.6 ± 2.6 |
| 5.65 – 6.56 | 41.4 ± 5.2 | 112.3 ± 8.5 | 17.7 ± 1.8 | 20.2 ± 3.3 | 27.5 ± 3.5 |
| 6.56 – 7.49 | 35.2 ± 4.2 | 99.8 ± 6.9 | 35.8 ± 2.8 | 24.8 ± 3.2 | 25.9 ± 3.1 |
| 7.49 – 8.26 | 29.5 ± 4.2 | 104.6 ± 8.0 | 40.0 ± 3.0 | 26.4 ± 3.6 | 24.0 ± 3.6 |
| 8.26 – 9.02 | 32.8 ± 4.5 | 95.3 ± 7.6 | 50.6 ± 3.5 | 34.5 ± 4.2 | 17.5 ± 3.6 |
| 9.02 – 9.90 | 22.7 ± 5.0 | 100.5 ± 8.0 | 54.9 ± 4.4 | 40.1 ± 4.3 | 17.4 ± 3.4 |
| 9.90 – 10.56 | 30.1 ± 5.7 | 98.6 ± 8.3 | 72.8 ± 6.5 | 38.5 ± 4.4 | 22.8 ± 4.6 |
| 10.56 – 11.28 | 18.2 ± 4.8 | 112.7 ± 9.7 | 70.5 ± 4.7 | 51.0 ± 6.1 | 16.8 ± 5.0 |
| 11.28 – 12.09 | 17.3 ± 6.5 | 102.4 ± 7.2 | 76.5 ± 4.9 | 47.4 ± 5.8 | 15.9 ± 5.1 |
| 12.09 – 12.98 | 20.4 ± 5.7 | 102.3 ± 6.6 | 78.0 ± 4.7 | 52.5 ± 5.7 | 17.9 ± 5.6 |
| 12.98 – 13.97 | 17.4 ± 5.4 | 65.8 ± 4.3 | 81.0 ± 4.3 | 60.0 ± 6.4 | 14.4 ± 5.5 |
| 13.97 – 15.09 | 6.2 ± 4.3 | 47.1 ± 3.8 | 73.1 ± 4.8 | 54.5 ± 5.6 | 10.2 ± 3.5 |
| 15.09 – 16.69 | 6.0 ± 2.6 | 26.6 ± 2.4 | 48.3 ± 3.5 | 30.1 ± 3.7 | |
| 16.69 – 18.55 | 5.7 ± 3.0 | 17.3 ± 2.5 | 27.8 ± 3.0 | | |
| 18.55 – 20.76 | | 16.3 ± 3.0 | 21.5 ± 3.0 | | |
| 20.76 – 22.82 | | 5.6 ± 2.9 | 11.7 ± 3.0 | | |
| 22.82 – 25.20 | | 5.7 ± 2.6 | 8.0 ± 2.4 | | |
| 25.20 – 27.99 | | 5.6 ± 2.7 | | | |
| 27.99 – 30.40 | | 5.2 ± 2.7 | | | |

[a] For incident neutron energy bin $4.20 \leq E_n \leq 4.71$ MeV.

The first entry in the third column of Table 5 for $E_\gamma = 1238$ keV illustrates an additional correction applied to a few of the measured cross sections. The threshold for this transition is 2.12 MeV, so that only a portion of the neutron flux in the given bin (of 1.68–2.36 MeV) contributes to the inelastic scattering reaction resulting in this transition. We computed the "active" portion of the flux (i.e., for $E_n = 2.12$ to 2.36 MeV) and used the recomputed flux for the determination of the cross section given in Table 5. The footnote to the entry is indicative that this correction was applied. Similar corrections were applied to other cross sections near threshold as indicated by appropriate footnotes, for example for $E_\gamma = 1811$ and 2113 keV in Table 5 and $E_\gamma = 2035$ keV in Table 6. Note that in Table 6 the first given energy bin has been slightly altered from the experimental bin limit given in Table 5. The lower limit of 3.18 MeV is the threshold energy for the first two transitions in Table 6; the alteration is in place of a footnote.

As mentioned above, for transitions having small cross sections (usually < 10 mb) sometimes we combined neutron-energy-binned groups to provide better defined peaks in the spectral data. Results obtained by combining two neutron-energy bins are first presented in Table 7. Cross sections obtained from the combined groupings are given in the last six rows following the cross section entries for the individual neutron-energy bins.

Entries in Tables 9, 12 and 14 are cross sections obtained after combining four neutron-energy-bin groups. The four groups are different for each of these three tables, however, since the cross sections for three different reactions are being tabu-

Table 7. Isotopic gamma-ray production cross sections (mb) associated with $^{56}Fe(n,p)^{56}Mn$ reactions

| Incident $E_n$ (MeV) | Gamma-ray energy (keV) of: | | | | | |
|---|---|---|---|---|---|---|
| | 212.0 | 335.5 | 314.4 | 454.3 | 271.1 | 541.4 |
| 3.18 – 3.83 | 0.82 ± 0.76 | | | | | |
| 3.83 – 4.71 | 0.80 ± 0.76 | | | | | |
| 4.71 – 5.65 | 1.15 ± 0.97 | | | | | |
| 5.65 – 6.56 | 2.80 ± 1.12 | | 1.72 ± 1.13 | | | |
| 6.56 – 7.49 | 6.61 ± 0.65 | | 3.5 ± 1.5 | | | |
| 7.49 – 8.26 | 10.15 ± 0.95 | 1.1 ± 2.2 | 4.7 ± 1.4 | | 3.0 ± 1.7 | |
| 8.26 – 9.02 | 9.67 ± 0.88 | 4.2 ± 2.2 | 6.56 ± 0.71 | | 7.0 ± 2.2 | 1.6 ± 0.9 |
| 9.02 – 9.90 | 12.9 ± 1.1 | 6.0 ± 2.6 | 4.9 ± 1.9 | | 8.4 ± 0.9 | 2.3 ± 1.2 |
| 9.90 – 10.56 | 14.8 ± 1.3 | 5.5 ± 2.7 | 8.10 ± 0.94 | 2.8 ± 3.4 | | |
| 10.56 – 11.28 | 15.9 ± 1.1 | 9.40 ± 0.95 | 11.40 ± 1.03 | 4.0 ± 3.2 | | |
| 11.28 – 12.09 | 16.6 ± 1.3 | 10.14 ± 0.95 | 9.57 ± 0.93 | 5.1 ± 2.4 | | |
| 12.09 – 12.98 | 16.6 ± 1.2 | 10.0 ± 2.1 | 11.79 ± 1.05 | | | |
| 12.98 – 13.97 | 17.1 ± 1.2 | 12.2 ± 1.0 | | | | |
| 13.97 – 15.09 | | 9.80 ± 0.92 | | | | |
| 15.09 – 16.69 | | 9.48 ± 0.82 | | | 4.2 ± 1.9 | |
| 16.69 – 18.55 | | 9.34 ± 0.83 | | | | |
| 18.55 – 20.76 | | 3.1 ± 3.0 | | | | |
| 20.76 – 22.82 | | 5.4 ± 2.8 | | | | |
| 22.82 – 25.20 | | 4.7 ± 2.9 | | | | |
| 9.90 – 11.28 | | | | | 7.8 ± 0.7 | 4.1 ± 2.6 |
| 11.28 – 12.98 | | | | | 5.8 ± 0.5 | 4.8 ± 2.5 |
| 12.98 – 15.09 | | | 8.16 ± 0.58 | 5.62 ± 0.58 | 4.7 ± 1.2 | 8.9 ± 0.8 |
| 15.09 – 18.55 | | | 6.13 ± 0.46 | 2.8 ± 2.0 | | 5.6 ± 0.6 |
| 18.55 – 22.82 | | | 3.00 ± 0.88 | 3.1 ± 2.1 | 1.2 ± 0.9 | 5.2 ± 2.3 |
| 22.82 – 27.99 | | | | | 2.9 ± 1.2 | 5.7 ± 3.8 |

lated. For each reaction the four groups were chosen to include the incident-neutron energy corresponding to the peak cross section for that reaction. As one may observe, the layout of these three tables is different from the other tables. Here the emphasis was on locating and quantifying transitions from all of the low- and intermediate-energy levels in the residual nucleus. Level excitation energies, transition energies and branching ratios were obtained from recent reports.[4,38] Corrections for sample absorption of gamma rays, neutron attenuation and multiple scattering were included, but time-slewing effects were not computed, the reason being that the timing intervals for each of the chosen four-bin groups were now large ($\geq$68 ns) compared to all but one of the measured timing resolutions discussed above. Any such corrections would, therefore, be expected to be small and likely well within the uncertainties associated with the other aspects of the data reduction. The remaining exception was for $E_\gamma = 126$ keV, and an average cross section for its appropriate four-bin group (Table 14) was not determined for this gamma ray.

More than 500 cross sections and associated uncertainties are tabulated in Tables 5–17. The uncertainties are total absolute uncertainties. More than half of the entries are for reactions and transitions observed for the first time and/or for incident neutron energies studied for the first time.

Table 8. Isotopic gamma-ray production cross sections (mb) associated with $^{56}$Fe$(n,\alpha)^{53}$Cr reactions

| Incident $E_n$ (MeV) | Gamma-ray energy (keV) of: | |
|---|---|---|
| | 1006.5 | 1289.6 |
| 12.98 – 13.97 | 12.5 ± 3.9 | |
| 13.97 – 15.09 | 13.3 ± 1.5 | |
| 15.09 – 16.69 | 11.6 ± 1.5 | 11.9 ± 1.4 |
| 16.69 – 18.55 | 12.4 ± 3.5 | 11.0 ± 1.4 |
| 6.55 – 8.26 | 0.7 ± 1.7 | 1.0 ± 1.6 |
| 8.26 – 9.90 | 5.7 ± 1.8 | 4.4 ± 1.8 |
| 9.90 – 11.28 | 6.0 ± 2.6 | 6.6 ± 2.5 |
| 11.28 – 12.98 | 8.1 ± 0.9 | 12.5 ± 1.2 |
| 12.98 – 15.09 | | 7.7 ± 2.3 |
| 18.55 – 22.82 | 7.3 ± 2.5 | 10.3 ± 1.1 |
| 22.82 – 27.99 | 8.0 ± 3.2 | 6.0 ± 2.4 |
| 27.99 – 33.15 | 1.2 ± 2.7 | 5.1 ± 2.3 |

Table 9. Average isotopic cross sections for $^{56}Fe(n,\alpha)^{53}Cr$ reactions for an incident neutron energy bin of 13.0 - 18.6 MeV

| $E_x^a$ (keV) | $E_\gamma^a$ (keV) | Branching Ratio[a] | $\sigma_\gamma^b$ (mb) |
|---|---|---|---|
| 564.1 | 564.1 | 1.0 | 4.7 ± 1.6 |
| 1006.5 | 1006.5 | 1.0 | 12.0 ± 0.7 |
| 1289.5 | 1289.5 | 0.935 | 10.4 ± 0.7 |
| 1536.7 | 530.2 | 0.65 | 6.9 ± 0.5 |
| | 247.1 | 0.26 | 1.5 ± 1.3 |
| 1973.6 | 1973.6 | 0.84 | 1.5 ± 1.4 |
| 2172.4 | 882.8 | 1.0 | 7.2 ± 0.7 |
| 2320.5 | 320.5 | 1.0 | 1.5 ± 1.5 |
| 2453.1 | 1446.8 | 0.45 | 2.2 ± 1.5 |
| 2655.8 | 1649.4 | 0.72 | 2.0 ± 1.4 |

[a]From Larson and Dickens, ref. 4.

[b]Corrected for sample absorption and multiple scattering but not for time slewing.

Table 10. Isotopic gamma-ray production cross sections (mb) associated with $^{56}Fe(n,2n)^{55}Fe$ reactions

| Incident $E_n$ (MeV) | Gamma-ray energy (keV) of: | | | | |
|---|---|---|---|---|---|
| | 411.3 | 931.3 | 1316.4 | 477.2 | 1408.3 |
| 12.09 - 12.98 | 6.3 ± 2.8 | | | | |
| 12.98 - 13.97 | 28.0 ± 4.0 | 23.2 ± 2.1 | 8.3 ± 3.8 | 8.0 ± 3.7 | 2.8 ± 3.4 |
| 13.97 - 15.09 | 32.5 ± 2.4 | 84.1 ± 7.4 | 53.7 ± 5.9 | 38.0 ± 4.3 | 23.7 ± 4.8 |
| 15.09 - 16.69 | 41.9 ± 2.2 | 185.8 ± 13.8 | 112.9 ± 9.6 | 67.6 ± 5.8 | 54.3 ± 7.6 |
| 16.69 - 18.55 | 46.3 ± 2.4 | 187.1 ± 7.6 | 147.8 ± 7.5 | 63.9 ± 3.0 | 49.4 ± 4.6 |
| 18.55 - 20.76 | 36.6 ± 3.2 | 188.9 ± 7.9 | 178.4 ± 8.1 | 66.2 ± 4.2 | 57.7 ± 3.5 |
| 20.76 - 22.82 | 33.7 ± 2.2 | 179.9 ± 8.7 | 176.0 ± 8.3 | 64.7 ± 3.3 | 57.8 ± 4.9 |
| 22.82 - 25.20 | | 153.1 ± 7.0 | 165.6 ± 8.0 | 54.1 ± 3.4 | |
| 25.20 - 27.99 | | 101.1 ± 7.1 | 106.2 ± 7.9 | 41.8 ± 2.8 | |
| 27.99 - 30.40 | | 68.7 ± 7.5 | 62.2 ± 9.9 | 33.9 ± 4.3 | |
| 30.40 - 33.15 | | 38.8 ± 6.9 | 44.1 ± 7.9 | 22.6 ± 4.1 | |
| 33.15 - 36.29 | | 33.5 ± 7.3 | 22.6 ± 5.3 | 17.4 ± 4.1 | |
| 36.29 - 38.64 | | 25.8 ± 5.6 | 16.1 ± 4.8 | | |
| 38.64 - 41.23 | | 17.0 ± 6.5 | 15.9 ± 5.0 | | |
| 36.29 - 41.23 | | | | 14.4 ± 2.9 | |

Table 11. Isotopic gamma-ray production cross sections (mb) associated with $^{56}Fe(n,2n)^{55}Fe$ reactions

| Incident $E_n$ (MeV) | Gamma-ray energy (keV) of: | | | |
|---|---|---|---|---|
| | 273.5 | 771.6 | 1222.5 | 1370.0 |
| 13.97 – 15.09 | 15.9 ± 3.6[a] | | 4.4 ± 2.5 | 3.7 ± 3.0 |
| 15.09 – 16.69 | 21.2 ± 2.6 | 3.2 ± 2.4 | 20.6 ± 2.1 | 15.9 ± 3.0 |
| 16.69 – 18.55 | 31.0 ± 1.7 | 10.2 ± 2.9 | 67.5 ± 5.2 | 28.1 ± 2.5 |
| 18.55 – 20.76 | 44.0 ± 3.4 | 12.3 ± 2.7 | 92.3 ± 5.3 | 26.3 ± 2.3 |
| 20.76 – 22.82 | 57.0 ± 4.5 | 16.9 ± 3.9 | 95.1 ± 5.3 | 26.6 ± 3.6 |
| 22.82 – 25.20 | 44.3 ± 3.6 | 14.7 ± 3.4 | 92.6 ± 5.2 | 29.8 ± 2.7 |
| 25.20 – 27.99 | 41.2 ± 3.8 | 9.2 ± 2.6 | 63.9 ± 4.6 | 26.0 ± 4.1 |
| 27.99 – 30.40 | 23.5 ± 1.9 | 8.8 ± 4.1 | 48.4 ± 5.5 | 17.6 ± 6.3 |
| 30.40 – 33.15 | 16.7 ± 3.0 | 11.0 ± 3.8 | 24.4 ± 4.7 | 11.5 ± 2.9 |
| 33.15 – 36.29 | 15.3 ± 3.3 | | 15.5 ± 4.0 | 9.4 ± 3.5 |
| 36.29 – 38.64 | | | 8.3 ± 3.6 | |
| 38.64 – 41.23 | | | 6.5 ± 3.3 | |
| 36.29 – 41.23 | | | 3.6 ± 3.4 | |

[a]For incident neutron energy bin $14.26 \leq E_n \leq 15.09$ MeV.

Table 12. Average isotopic gamma-ray production cross sections for $^{56}Fe(n,2n)^{55}Fe$ reactions for an incident neutron energy bin of 15.1 to 22.8 MeV

| $E_x^a$ (keV) | $E_\gamma^a$ (keV) | Branching Ratio[a] | $\sigma_\gamma^b$ (mb) |
|---|---|---|---|
| 411.8 | 411.8 | 1.0 | 38.3 ± 1.2 |
| 931.3 | 931.3 | 0.08 | 182 ± 5 |
| 1316.5 | 385.3 | 0.07 | 13.1 ± 0.6 |
| | 1316.5 | 0.93 | 147 ± 4 |
| 1408.4 | 477.2 | 0.53 | 64.7 ± 1.7 |
| | 1408.4 | 0.44 | 53.1 ± 1.8 |
| 1918.3 | 1507.1 | 0.32 | 2.0 ± 1.1 |
| | 1918.3 | 0.68 | 2.6 ± 1.0 |
| 2051.7 | 1640.5 | 0.77 | 0.0 ± 0.9 |
| | 2051.6 | 0.23 | 2.6 ± 1.5 |
| 2143.5 | 827.1 | 0.36 | 6.3 ± 1.6 |
| | 1213.0 | 0.43 | 5.5 ± 1.1 |
| | 2143.5 | 0.18 | 0.0 ± 1.3 |
| 2211.9 | 803.4[c] | 0.98 | 40 ± 10 |
| 2301.1 | 984.6 | 0.08 | 4.6 ± 1.0 |
| | 1369.7 | 0.92 | 24.2 ± 1.6 |
| 2470.2 | 2058.4 | 0.34 | 0.4 ± 1.3 |
| | 2470.2 | 0.66 | 2.8 ± 1.3 |
| 2539.1 | 1222.5 | 0.97 | 64.0 ± 2.9 |
| 2813.8 | 274.8[d] | 1.0 | 33.1 ± 1.0 |
| 2872.3 | 1556.0 | 0.25 | 2.0 ± 1.3 |
| 2938.9 | 1622.3 | 0.45 | 1.0 ± 1.0 |
| 2984.4 | 771.6 | | 12.7 ± 1.7 |
| | 1576.0 | | 2.9 ± 1.2 |
| 3072.0 | 532.5 | 0.83 | 5.4 ± 1.0 |
| 3108.7 | 1792.1 | 0.22 | 1.3 ± 1.4 |
| | 2177.6 | 0.76 | 1.1 ± 1.5 |

[a] From evaluation of Zhou, et al., ref. 37.

[b] Corrected for sample absorption and multiple scattering but not for time slewing.

[c] Coincident with background radiation [$^{206}Pb(n,n'\gamma)$]. An estimate was made of the background contribution, and the uncertainty reflects the difficulty of this estimation.

[d] $E_\gamma = (273.5 \pm 0.5)$ keV measured in the present experiment. This gamma ray lies close to, and was resolved from, the $E_\gamma = 271$ keV due to a transition in $^{56}Mn$.

Table 13. Isotopic gamma-ray production cross sections (mb) associated with $^{56}Fe(n, d + n, np)^{55}Mn$ reactions

| Incident $E_n$ (MeV) | Gamma-ray energy (keV) of: | | |
|---|---|---|---|
| | 125.95 | 858.2 | 1166.3 |
| 9.90 – 10.56 | 0.2 ± 2.0 | | |
| 10.56 – 11.28 | 0.7 ± 3.3 | | |
| 11.28 – 12.09 | 29.4 ± 15.0 | | |
| 12.09 – 12.98 | 44.5 ± 6.5 | | |
| 12.98 – 13.97 | 62.9 ± 3.6 | | |
| 13.97 – 15.09 | 91.6 ± 5.9 | | |
| 15.09 – 16.69 | 93.7 ± 6.0 | 21.1 ± 4.8 | 5.6 ± 2.9 |
| 16.69 – 18.55 | 110.5 ± 11.9 | 31.3 ± 5.3 | 19.0 ± 1.9 |
| 18.55 – 20.76 | 114 ± 18 | 35.4 ± 4.3 | 22.5 ± 3.0 |
| 20.76 – 22.82 | 131 ± 34 | 42.8 ± 4.3 | 25.7 ± 3.2 |
| 22.82 – 25.20 | 122 ± 31 | 48.4 ± 6.1 | 41.1 ± 3.2 |
| 25.20 – 27.99 | 101 ± 26 | 45.1 ± 6.1 | 33.6 ± 2.8 |
| 27.99 – 30.40 | 72 ± 18 | 46.3 ± 6.2 | 28.5 ± 5.5 |
| 30.40 – 33.15 | 72 ± 22 | 27.5 ± 4.6 | 35.5 ± 3.9 |
| 33.15 – 36.29 | 53.1 ± 16.5 | 17.9 ± 3.6 | 17.9 ± 5.3 |
| 36.29 – 38.64 | | 7.2 ± 4.2 | 19.9 ± 5.4 |
| 38.64 – 41.23 | | | 11.1 ± 5.4 |

Table 14.
Average isotopic gamma-ray production cross sections for $^{56}Fe(n, d + n, np)^{55}Mn$ reactions for an incident neutron energy bin of 18.6 to 28.0 MeV

| $E_x^a$ (keV) | $E_\gamma^a$ (keV) | Branching Ratio[a] | $\sigma_\gamma^b$ (mb) |
|---|---|---|---|
| 984.29 | 858.2 | 0.95 | 42.8 ± 2.2 |
| 1292.18 | 308.1 | 0.20 | 10.0 ± 0.7 |
| | 1166.3 | 0.80 | 28.1 ± 1.9 |
| 1293.0 | 1293.0 | 1.0 | 4.3 ± 1.6 |
| 1528.37 | 1528.3 | 0.97 | 6.8 ± 1.4 |
| 2198.38 | 2198.5 | 0.61 | 3.0 ± 1.7 |
| 2311.52 | 1019.42 | 0.90 | 8.3 ± 0.7 |

[a]From evaluation of Zhou, et al., ref. 37.

[b]Corrected for sample absorption and multiple scattering, but not for time slewing.

Table 15. Isotopic gamma-ray production cross sections (mb) associated with $^{56}Fe(n,n\alpha)^{52}Cr$ reactions

| Incident $E_n$ (MeV) | Gamma-ray energy (keV) of: | | | |
|---|---|---|---|---|
| | 1434.1 | 935.5 | 1333.6 | 744.2 |
| 18.55 – 20.76 | 26.0 ± 3.9 | 11.5 ± 3.0 | | |
| 20.76 – 22.82 | 41.5 ± 5.5 | 19.1 ± 3.7 | | |
| 22.82 – 25.20 | 51.1 ± 6.2 | 20.6 ± 3.8 | 19.5 ± 2.3 | 5.6 ± 4.0 |
| 25.20 – 27.99 | 60.9 ± 6.2 | 20.7 ± 4.4 | 25.3 ± 4.5 | 13.6 ± 4.1 |
| 27.99 – 30.40 | 49.9 ± 5.5 | 27.8 ± 5.0 | | 21.9 ± 4.6 |
| 30.40 – 33.15 | 35.8 ± 5.7 | 26.2 ± 5.8 | | 12.9 ± 4.2 |
| 33.15 – 36.29 | 34.1 ± 5.6 | 22.9 ± 5.0 | | |
| 36.29 – 38.64 | 24.5 ± 6.0 | 19.2 ± 8.3 | | |
| 12.98 – 15.09 | 2.9 ± 2.0 | | | |
| 15.09 – 18.55 | 7.7 ± 2.0 | 3.2 ± 1.8 | 2.1 ± 1.9 | |
| 18.55 – 22.82 | | | 10.6 ± 4.9 | |
| 27.99 – 33.15 | | | 18.2 ± 3.2 | |
| 33.15 – 38.64 | | | 9.7 ± 3.1 | 10.2 ± 3.2 |

Table 16. Isotopic gamma-ray production cross sections (mb) associated with $^{56}Fe(n,3n)^{54}Fe$ reactions

| Incident $E_n$ (MeV) | Gamma-ray energy (keV) of: | | |
|---|---|---|---|
| | 1408.1[a] | 1129.9 | 756.6 |
| 22.82 – 25.20 | 0.4 ± 5.9 | 2.9 ± 3.6[b] | |
| 25.20 – 27.99 | 23.7 ± 6.2 | 9.5 ± 2.5 | 3.6 ± 4.0 |
| 27.99 – 30.40 | 58.1 ± 8.5 | 44.7 ± 6.7 | |
| 30.40 – 33.15 | 78.9 ± 9.2 | 58.4 ± 6.8 | |
| 33.15 – 36.29 | 92.7 ± 9.3 | 68.2 ± 6.7 | |
| 36.29 – 38.64 | 77.2 ± 12.0 | 44.3 ± 7.6 | |
| 38.64 – 41.23 | 53.0 ± 13.6 | 18.8 ± 7.7 | |
| 27.99 – 33.15 | | | 7.5 ± 3.7 |
| 33.15 – 38.64 | | | 10.8 ± 1.7 |

[a] See Table 2.

[b] For incident neutron energy bin $23.45 \leq E_n \leq 25.20$ MeV.

Table 17. Isotopic gamma-ray production cross sections (mb) associated with $^{56}\mathrm{Fe}(n, t + n, nd + n, 2np)^{54}\mathrm{Mn}$ reactions

| Incident $E_n$ (MeV) | Gamma-ray energy (keV) of: | | | |
|---|---|---|---|---|
| | 156.2 | 211.6 | 705.4 | 251.3 |
| 15.09 – 16.69 | 1.4 ± 3.2 | | | |
| 16.69 – 18.55 | 9.8 ± 6.2 | 3.9 ± 2.8 | | |
| 18.55 – 20.76 | 17.4 ± 3.1 | 8.5 ± 1.9 | | |
| 20.76 – 22.82 | 19.4 ± 2.9 | 9.2 ± 1.8 | | |
| 22.82 – 25.20 | 22.9 ± 2.6 | 18.2 ± 2.0 | 5.6 ± 3.0 | |
| 25.20 – 27.99 | 37.2 ± 2.8 | 33.8 ± 3.2 | 8.0 ± 4.0 | |
| 27.99 – 30.40 | 80.4 ± 12.9 | 42.8 ± 4.9 | 30.3 ± 6.9 | |
| 30.40 – 33.15 | 82.1 ± 14.1 | 69.6 ± 9.0 | 41.8 ± 9.2 | |
| 33.15 – 36.29 | 92 ± 20 | 71.8 ± 10.1 | 42.6 ± 6.5 | |
| 36.29 – 38.64 | 107 ± 33 | 85 ± 16 | 53.8 ± 7.9 | |
| 38.64 – 41.23 | 144 ± 69 | 96 ± 25 | 70.4 ± 9.9 | |
| 20.76 – 25.20 | | | | 0.4 ± 1.1 |
| 25.20 – 30.40 | | | | 4.2 ± 2.2 |
| 30.40 – 36.29 | | | | 9.4 ± 3.1 |
| 36.29 – 41.23 | | | | 6.6 ± 1.3 |

# 4. DISCUSSION OF THE DATA

The primary purpose of this report is to archive the experimental gamma-ray production cross sections for future reference. Hence, this section will not include a complete analysis of these data. Indeed, as mentioned above, we were primarily interested in the nonelastic events rather than the inelastic events, and we reduced only the largest-yield data for the latter primarily to establish a kind of a fiduciary to determine the adequacy of the experimental technique and data reduction for the data of interest.

In Fig. 4 are shown the present gamma-ray production cross sections for $E_\gamma =$ 847 keV, the principal gamma ray from inelastic scattering, compared with some, but not all, of the earlier experiments. The results in this figure are given in isotopic cross sections; the elemental cross sections reported in the earlier experiments have been normalized using the elemental abundance of $^{56}$Fe in natural iron of 91.8%. In addition, for $E_n > 10$ MeV, the earlier data have to be corrected for the contribution from the minor isotope $^{57}$Fe (2.1% abundance in elemental iron). This correction was computed using measured $^{57}$Fe$(n, 2n\gamma)$ gamma-ray production cross sections.[1] One difficulty with comparison with earlier measurements is that high resolution (in incident neutron energy) measurements of the 847-keV gamma-ray production cross section[16,18] shows considerable resonance-like structure even for $E_n \sim 6$ MeV (these data are not shown in Fig. 4), and so experiments using monoenergetic neutron sources may result in rather different cross sections than the present data since the present data provide an *average* cross section for the incident neutron energy interval. The present data agree within ±20% uncertainties with data reported by Benjamin, Buchanan and Morgan[13] (not shown in Fig. 4) except for $E_n = 1.5$ MeV. The present data are also in good agreement with earlier ORNL elemental cross section data[8] obtained with a NaI-based detector system for $E_n < 4$ MeV for the experimental gamma-ray energy bin 0.71–0.95 MeV. For this same incident neutron energy region, however, as shown in Fig. 4, our present results are definitely smaller than the IRT data.[10] The Obninsk cross-section data[15] (not shown in Fig. 4; but see, however, Fig. 12 of ref. 8 for a comparison of the Obninsk data with the prior ORNL results) exhibit substantial dependence on incident neutron energy; these data, however, appear to be in agreement with the trend of the excitation function for $E_n$ between 1 and 6 MeV. Finally, for $E_n \sim 15$ MeV the Lund measurement[14] and the Beijing Normal University measurement[19] (neither are shown on Fig. 4) are ~2 times larger than deduced from the present data. The present data agree with the IRT measurements[10] over the incident neutron energy region from 4 to 12 MeV. Our data are ~10% smaller than data obtained at Studsvik[11] for $E_n$ between 16 and 18 MeV. We have no explanation for the sudden increase in this cross section previously reported[11] for $E_n > 20$ MeV; our data continue the trend toward smaller values, a trend likely more in line with physical expectations.

Comparisons of our data with a representation of earlier measurements for $E_\gamma = 1238$ keV are shown in Fig. 5. Agreement with the IRT data[10] seems a little better than shown in Fig. 4 for $E_\gamma = 847$ keV except perhaps for $E_n$ between 10 and 13 MeV. Indeed, the data sets exhibited in Fig. 5 tend to show very reasonable agreement, at least to within the various stated uncertainties. Previous experimental results not shown in Fig. 5 include the LANL data[6] for $E_n$ between

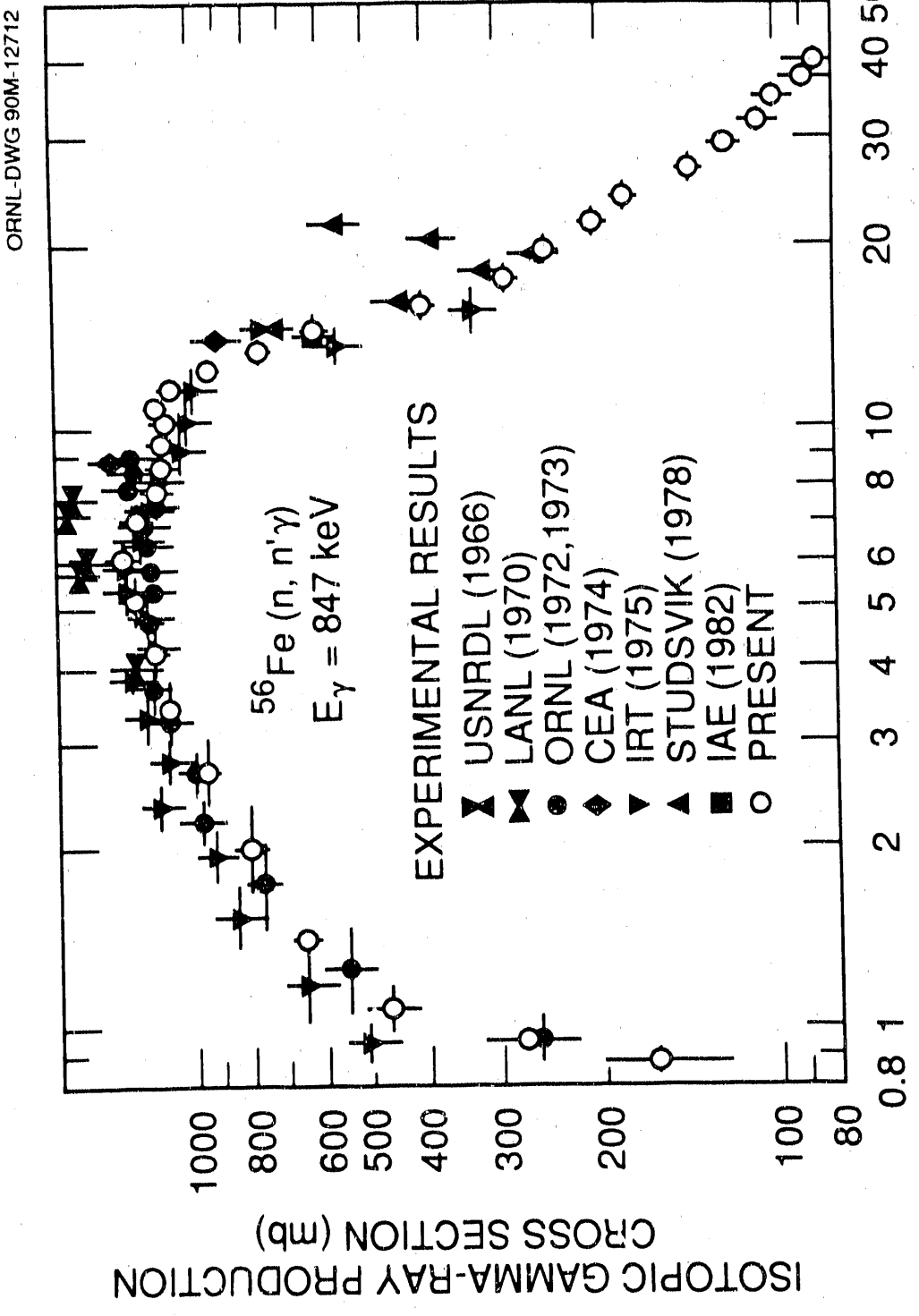


**Fig. 4. Isotopic cross sections for the production of the 847-keV gamma ray.** The present data (open circles) are compared with previous measurements (solid symbols) given as follows: USNRDL, ref. 5; LANL, ref. 6; ORNL, refs. 7 and 8; CEA, ref. 9; IRT, ref. 10; Studsvik, ref. 11; and IAE (Beijing), ref. 12.

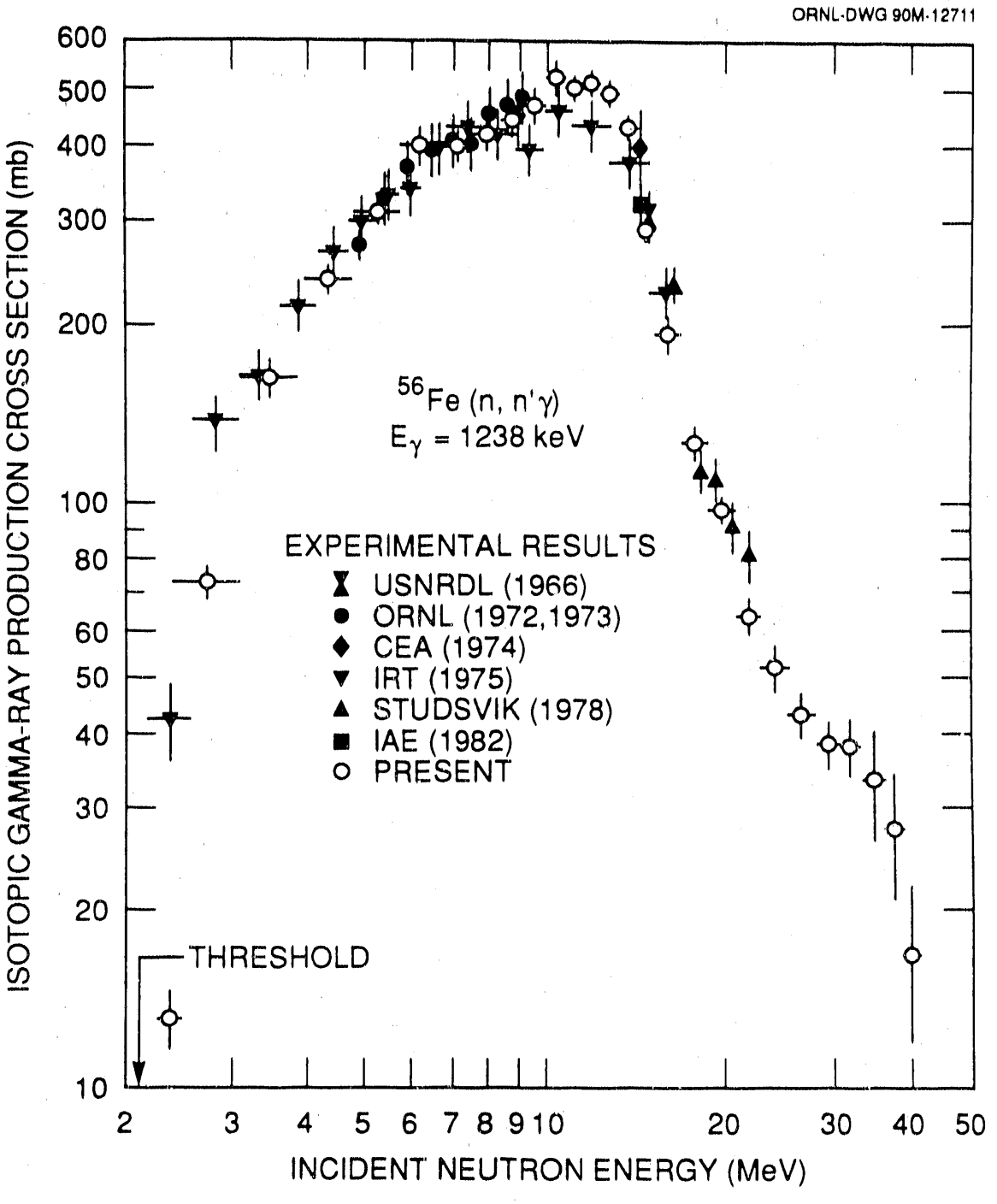


**Fig. 5. Isotopic cross sections for the production of the 1238-keV gamma ray.** The present data (open circles) are compared with previous measurements (solid symbols) given as follows: USNRDL, ref. 5; ORNL, refs. 7 and 8; CEA, ref. 9; IRT, ref. 10; Studsvik, ref. 11; and IAE (Beijing), ref. 12.

4 and 8 MeV which are ~50% larger than the present results; the Beijing Normal University datum[19] at $E_n = 14.9$ MeV which is also about 50% larger than present results; and the Lund datum[14] at $E_n = 15.1$ MeV which agrees to within its assigned 15% uncertainty with the present data. One may also note that the Studsvik data[11] for $E_n > 20$ MeV do not increase with increasing $E_n$ in a manner similar to that shown in Fig. 4 for $E_\gamma = 847$ keV but rather follow the trend of the present data.

Comparisons for other $^{56}$Fe$(n, n'\gamma)$ transitions were studied. These comparisons are, for the most part, as favorable as for $E_\gamma = 1238$ keV; however, the uncertainties assigned to all data sets are larger, and so the comparisons tend to indicate "better" agreement simply on the basis of the overlap of error bars.

As mentioned in the Introduction, the emphasis for this experiment was in the study of gamma radiation due to tertiary reactions. Of these reactions, previous experiments[5,10–12,14,19] reported cross sections for discrete-transition gamma rays from $^{56}$Fe$(n, 2n\gamma)^{55}$Fe reactions. The present isotopic gamma-ray production cross sections for $E_\gamma = 931$ keV are exhibited in Fig. 6 compared to earlier measurements of cross sections for this gamma ray, and for $E_\gamma = 1316$ keV in Fig. 7 also compared to earlier measurements. The IRT values appear to be much too large for $E_n$ close to threshold but in good agreement for the next larger $E_n$ bin. The IAE[12] data agree well for both transitions. The Beijing Normal University[19] data (not shown in these figures), however, are ≈10 times too big. The Studsvik[11] measurements are rather interesting, being smaller for $E_n \sim 16$ and 18 MeV, and a little larger for $E_n \sim 19$ and 20 MeV. We do not wish to suggest an error in their beam-energy measurements, only to observe that if all of their $E_n = 16.1$ MeV data points were replotted at $E_n \sim 15$ MeV, there would be very good agreement with the present measurements for the four gamma-ray excitation functions shown in Figures 4–7.

We remark in closing this Discussion that we obtained our cross section values and uncertainties using standard methods. We have carefully reviewed all aspects of our experiment, including not only the data reduction but also all of the corrections that were necessary. Comparisons with earlier measurements (Figures 4–7) are not meant to "validate" the present data because no set of measurements provides a complete picture of the $n+$ $^{56}$Fe interaction. The cross sections reported herein are as accurate as can be provided within the framework of our experimental system. What these measurements will do is to provide data to guide a consistent nuclear-model development and computations of the type, for example, used to prepare the recent ENDF evaluation for iron,[30] not only for current evaluation efforts for $E_n \leq 20$ MeV but potential future efforts for $E_n > 20$ MeV.

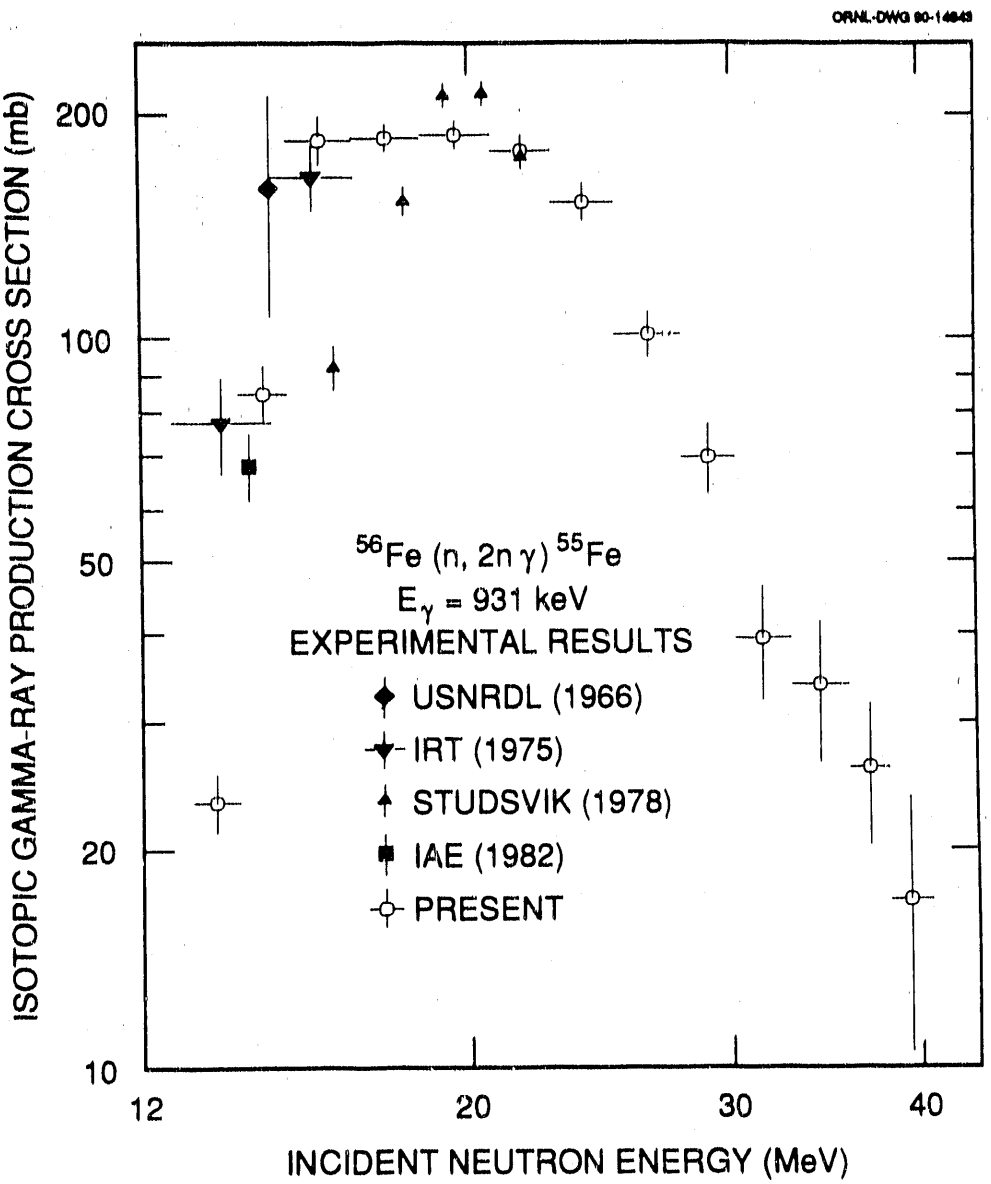


**Fig. 6. Isotopic cross sections for the production of 931-keV gamma ray.** The present data (open circles) are compared with previous measurements (solid symbols) given as follows: USNRDL, ref. 5; IRT, ref. 10; Studsvik, ref. 11; and IAE (Beijing), ref. 12.

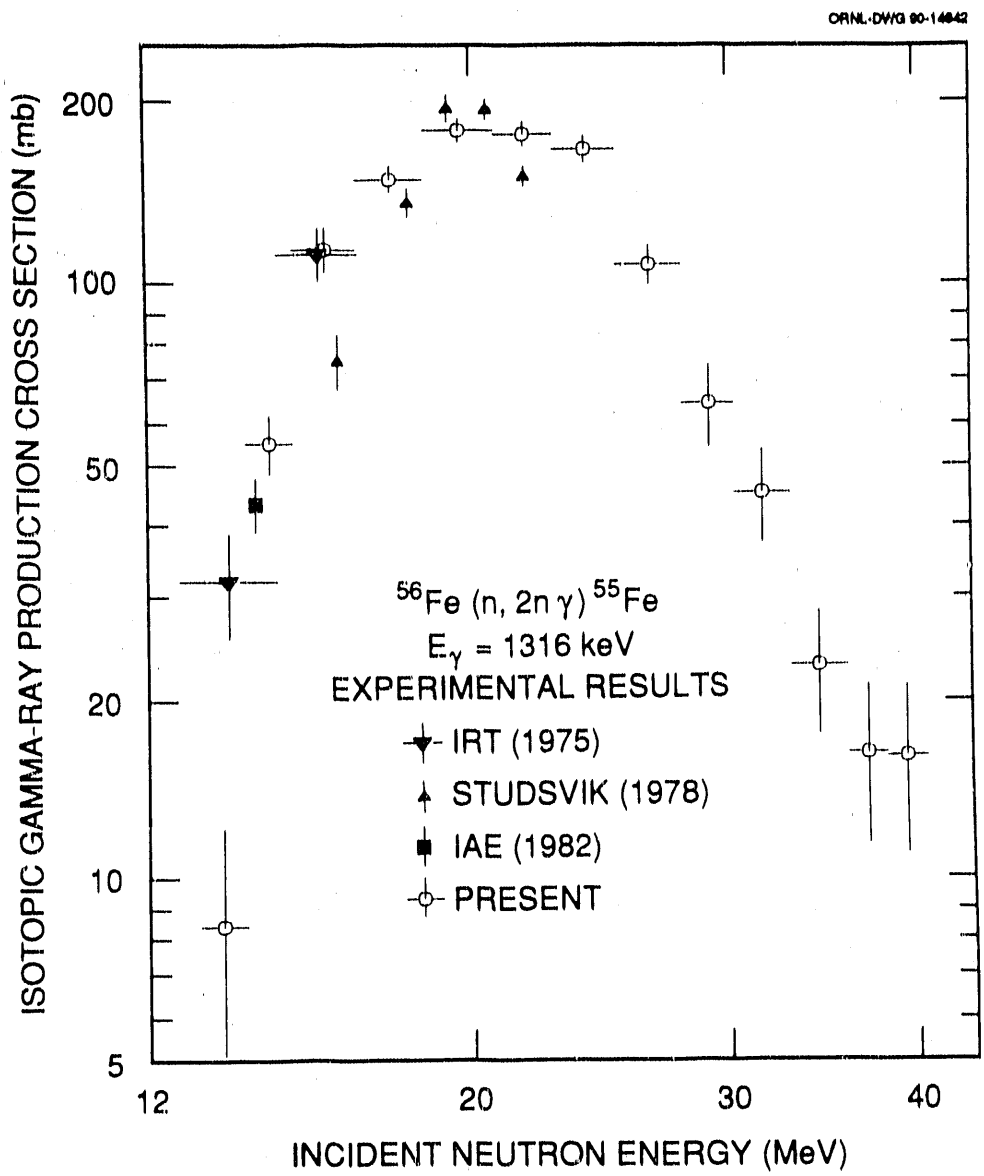


**Fig. 7. Isotopic cross sections for the production of the 1316-keV gamma ray.** The present data (open circles) are compared with previous measurements (solid symbols) given as follows: IRT, ref. 10; Studsvik, ref. 11; and IAE (Beijing), ref. 12.

# REFERENCES


1. Z. W. Bell, J. K. Dickens, J. H. Todd and D. C. Larson, *Nucl. Sci. Engr.* **84**, 12 (1983).
2. J. K. Dickens and D. C. Larson, *Gamma-ray Decay of Levels in* $^{53}Cr$, ORNL-6418 (1987).
3. J. K. Dickens and D. C. Larson, "$^{10,11}$B$(n,x\gamma)$ Reactions for Incident Neutron Energies Between 0.1 and 25 MeV," in *Nucl. Data for Sci. and Tech.*, Mito (Japan) May 30 - June 3, 1988, ed. S. Igarasi (Saikon Publ. Co. Ltd., Tokyo, 1988) p. 213.
4. D. C. Larson and J. K. Dickens, *Phys. Rev. C* **39**, 1736 (1989).
5. F. C. Engesser and W. E. Thompson, *J. Nucl. Engr.* **21**, 487 (1967).
6. D. M. Drake, J. C. Hopkins and C. S. Young, *Nucl. Sci. Engr.* **40**, 294 (1970).
7. J. K. Dickens, G. L. Morgan and F. G. Perey, *Gamma-ray Production Due to Neutron Interactions with Iron for Incident Neutron Energies Between 0.8 and 20 MeV: Tabulated Differential Cross Sections*, ORNL-4798 (1972)
8. J. K. Dickens, G. L. Morgan and F. G. Perey, *Nucl. Sci. Engr.* **50**, 311 (1973).
9. J. Lachkar, J. Sigaud, Y. Patin and G. Haouat, *Nucl. Sci. Engr.* **55**, 168 (1974).
10. V. J. Orphan, C. G. Hoot and V. C. Rogers, *Nucl. Sci. Engr.* **57**, 309 (1975).
11. V. Corcalciuc, B. Holmqvist, A. Marcinkowski and G. A. Prokopets, *Nucl. Phys.* **A307**, 445 (1978).
12. Shi Xia-Min, Shen Rong-Lin, Xing Jin-Qiang and Din Da-Zhao, *Chinese J. Nucl. Phys.* **4**(2) 120 (1982).
13. R. W. Benjamin, P. S. Buchanan and I. L. Morgan, *Nucl. Phys.* **79**, 241 (1966).
14. B. Jonsson, K. Nyberg and I. Berqvist, *Arkiv Fys.* **39**, 295 (1968).
15. D. L. Broder, A. P. Gamaly, A. N. Lashchuk and Y. P. Sadokhin, "Nuclear Data for Reactors," in *Proc. 2nd Int. Conf. Nucl. Data for Reactors*, Helsinki, June 1970, Int. At. Energy Agency, Vienna (1970), p. 295.
16. F. Voss, "Messung und Fluktuationsanalyse von $\gamma$-Produktionsquer-schnitten nach inelastischer Neutronenstreuung an $^{56}$Fe und $^{27}$Al zwischen 0.8 und 13 MeV," Dissertation, Karlsruhe Univ. (1972).
17. G. Grenier, "Sections Efficaces de Production de Rayonnement Gamma pour le Magnesium, le Silicium, le Calcium, le Scandium, le Chrome, le Nickel et le Fer Natural avec des Neutrons de 14.1 MeV," in *Nat. Sov. Conf. on Neutron Phys*, Kiev, May 28 - June 1, 1973 (1973).
18. J. D. Kellie, M. N. Islam and G. I. Crawford, *Nucl. Phys.* **A208**, 525 (1973).
19. Zhou Hongyu, Tang Lin, Yan Yiming, Wen Shenlin, Lan Liquiao, Zhan Shenji, Wang Qi, Sun Shuxu, Han Chongzhan, Ding Xiaoji and Wang Wanhong, *Gamma Ray Production Cross Sections for the Interactions of 14.9-MeV Neutrons with C, Al, V, Fe and Nb at 90 Degrees*, Int. At. Energy Agency report INDC(CPR)-10, 8611 (1986). The data are available in the CINDA compilation, entry no. 30904001 *ff*.

20. G. L. Morgan, T. A. Love and F. G. Perey, *Nucl. Instr. Meth.* **128**, 125 (1975). See also K. H. Bockhoff, A. D. Carlson, O. A. Wasson, J. A. Harvey and D. C. Larson, *Nucl. Sci. Engr* (in press, 1990).

21. R. G. Alsmiller, Jr., T. A. Gabriel, and M. P. Guthrie, *Nucl. Sci. Engr.* **40**, 365 (1970).

22. Z. W. Bell, J. K. Dickens, J. H. Todd and D. C. Larson, *Neutron Flux Measurements at the 22-meter Station of the Oak Ridge Electron Linear Accelerator Flight Path No. 8*, ORNL/TM-8514 (1983).

23. J. K. Dickens, *SCINFUL: A Monte-Carlo-Based Computer Program to Determine a Scintillator Full Energy Response to Neutron Detection for $E_n$ Between 0.1 and 80 MeV: User's Manual and FORTRAN Program Listing*, ORNL-6462 (1988).

24. R. E. Textor and V. V. Verbinski, *O5S: A Monte Carlo Code for Calculating Pulse Height Distributions due to Monoenergetic Neutrons Incident on Organic Scintillators*, ORNL-4160 (1968).

25. In the actual experiment there were several experimental spectra obtained for $E_n < 0.8$ MeV; however, no peaks of interest were observed in these spectra. In addition, a spectrum was obtained for $E_n > 41$ MeV, but the background was too large for reliable data reduction.

26. J. G. Craven, *OPRODF, A Decsystem-10 Data Manipulation Program for ORELA Data Formatted Files*, ORNL/CSD/TM-45 (1978). OPRODF became FORODF as used on the VAX 11/785.

27. Written by Z. W. Bell (1983).

28. A modification of the code TPASS by Z. W. Bell (1983). See J. K. Dickens, *TPASS, A Gamma-ray Spectrum Analysis and Isotope Identification Computer Code*, ORNL-5732 (1982).

29. R. L. Bywater, Jr., *Gamma-ray Production Cross Sections for 0.9 to 20 MeV Neutron Interactions with $^{10}B$*, ORNL/TM-10191 (1986).

30. E. Storm and H. I. Israel, *Nucl. Data Tables* **A7**, 565 (1970).

31. C. Y. Fu, D. M. Hetrick, F. G. Perey and C. M. Perey (unpublished, 1990); for supporting documentation see also C. Y. Fu and D. M. Hetrick, *Update of ENDF/B-V Mod-3 Iron: Neutron Producing Reaction Cross Sections and Energy-Angle Correlations*, ORNL/TM-9964(ENDF-341) (1986); C. Y. Fu, D. M. Hetrick, C. M. Perey, F. G. Perey, N. M. Larson and D. C. Larson, "Improvements in ENDF/B-V Iron and Possible Impacts on Pressure Vessel Surveillance Dosimetry," in *Seventh ASTM Euratom Symposium on Reactor Dosimetry*, Strasbourg, Aug. 25-30, 1990 (to be published).

32. E. D. Arthur and P. G. Young, *Evaluated Neutron-induced Cross Sections for $^{54,56}Fe$ to 40 MeV*, LA-8626-MS(ENDF-304) (1980).

33. Huo Junde, Hu Dailing, Zhou Chunmei, Han Xiaoling, Hu Baohua and Wu Yaodong, *Nucl. Data Sheets* **51**, 1 (1987).

34. R. B. Day, *Phys. Rev.* **102**, 767 (1956); G. L. Morgan and F. G. Perey, *Nucl. Sci. Engr.* **61**, 337 (1976).

35. S. Bose, M. B. Chatterjee, B. K. Sinha and R. Bhattacharya, **Nucl. Instr. Meth. A254**, 79 (1987); *ibid.*, **A254**, 118 (1987).

36. T. J. Paulus, T. W. Raudorf, B. Coyne and R. Trammell, *IEEE Trans. Nucl. Sci.* NS-28, 544 (1981); C. L. Britton, T. H. Becker, T. J. Paulus and R. C. Trammell,*ibid.,* NS-31, 454 (1984).

37. Similar to calculations for a closed-end diode by A. Alberigi-Quaranta, A. Catellani, G. Pizziolo and G. Zaraini, *IEEE Trans. Nucl. Sci.* NS-31, 900 (1984).

38. Zhao Enchen, Huo Junde, Zhou Chunmei, Lu Xiane and Wang Lizheng, *Nucl. Data Sheets* 44, 463 (1985).

# -END-

# DATE FILMED

11 / 1 / 90